

**Experimental study on the nucleate boiling heat transfer characteristics of a water-based multi-walled carbon nanotubes nanofluid in a confined space**

XIA, Guodong, DU, Mo, CHENG, Lixin and WANG, Wei

Available from Sheffield Hallam University Research Archive (SHURA) at:

<http://shura.shu.ac.uk/15875/>

---

This document is the author deposited version. You are advised to consult the publisher's version if you wish to cite from it.

**Published version**

XIA, Guodong, DU, Mo, CHENG, Lixin and WANG, Wei (2017). Experimental study on the nucleate boiling heat transfer characteristics of a water-based multi-walled carbon nanotubes nanofluid in a confined space. *International Journal of Heat and Mass Transfer*, 113, 59-69.

---

**Copyright and re-use policy**

See <http://shura.shu.ac.uk/information.html>

1 **Experimental study on the nucleate boiling heat transfer characteristics of a**  
2 **water-based multi-walled carbon nanotubes nanofluid in a confined space**

3 Guodong Xia<sup>a,\*</sup>, Mo Du<sup>a</sup>, Lixin Cheng<sup>a,b</sup>, Wei Wang<sup>a</sup>

4  
5 <sup>a</sup>Key Laboratory of Enhanced Heat Transfer and Energy Conservation, Ministry of Education,  
6 College of Environmental and Energy Engineering, Beijing University of Technology, Beijing  
7 100124, China

8 <sup>b</sup>Department of Engineering and Mathematics, Faculty of Arts, Computing, Engineering and  
9 Science, Sheffield Hallam University, City Campus, Howard Street, Sheffield, S1 1WB, UK

10  
11 **Abstract:** Experimental investigation of nucleate boiling heat transfer of a **water-based**  
12 **multi-walled carbon nanotubes** (MWCNTs) nanofluid in a confined space is presented in this  
13 study. First, the effects of four different surfactants on the stability of the nanofluids were  
14 investigated and the suitable surfactant gum acacia (GA) was selected for the boiling  
15 experiments. Then, the boiling experiments of the nanofluids with various volume fractions  
16 (0.005% - 0.2%) of the MWCNTs were conducted at a sub-atmospheric pressure of  $1 \times 10^{-3}$  Pa  
17 and the test heat fluxes are from 100 to 740 kW/m<sup>2</sup>. Furthermore, GA with four different mass  
18 fractions was respectively dissolved in the nanofluids to investigate the effect of the GA  
19 concentration on the boiling heat transfer. The effects of the heat flux, the concentrations of the  
20 MWCNTs and surfactants, the bubble behaviors and the surface conditions after the boiling  
21 processes have been analyzed. The results show that the MWCNTs nanofluid can enhance  
22 boiling heat transfer as compared to the base fluid. This is mainly caused by the nanoparticles  
23 deposition on the boiling surface result in increasing the surface roughness and reducing surface  
24 contact angle. It is also found that addition of GA can inhibit the deposition of the nanoparticles  
25 but may reduce the boiling heat transfer coefficient of the nanofluids. According to the

26 experimental results, the maximum heat transfer coefficient enhancement ratio can reach 40.53%.  
27 It is also noticed that the heat transfer enhancement ratio decreases with increasing the heat flux  
28 at lower heat fluxes from 100 to 340 kW/m<sup>2</sup> while it increases with increasing the heat flux at  
29 higher fluxes from 340 to 740 kW/m<sup>2</sup>. At the lower heat fluxes, the deposition layer increases the  
30 frequency of bubble formation and thus the boiling heat transfer is strengthened. While at the  
31 high heat fluxes, the increasing heat flux may strengthen the capability of the nanoparticles  
32 deposition and the disturbance of the nanoparticles and increase the enhancement ratio of heat  
33 transfer coefficient.

34 **Keywords:** nanofluids, MWCNTs, nucleate boiling, heat transfer, enhancement, mechanism

35

## 36 **1. Introduction**

37 As a new type of heat transfer medium, nanofluids have been attracting tremendous  
38 attention in the field of thermal science and engineering in recent years due to their high thermal  
39 conductivity, unique colloidal property and heat transfer behaviors [1-8]. Numerous researchers  
40 have conducted investigation into the heat transfer enhancement including single phase and  
41 phase change heat transfer using nanofluids [9-20]. In particular, the nucleate boiling heat  
42 transfer characteristics in confined spaces are of great interest to removing high heat flux in the  
43 microelectronic system, **laser devices, green and highly efficient lighting** with limited cooling  
44 spaces. Although a large number of researchers have investigated on the pool boiling heat  
45 transfer characteristics with plenty kinds of nanofluids in unconfined spaces, there lacks study of  
46 the characteristics of nucleate boiling heat transfer using the multi-walled carbon nanotubes  
47 (MWCNTs) nanofluid in confined spaces at sub-atmospheric pressures. Therefore, it is essential  
48 to conduct experimental investigation on the relevant topic.

49 Nanofluids which possess application prospects in the heat transfer field were firstly

50 proposed by Choi [1] in 1995. From then on, numerous studies of heat transfer of nanofluids  
51 have been conducted to understand and explore their fundamentals and applications. The  
52 suspension stability and thermal conduction mechanism of nanofluids were studied by Xuan et al.  
53 [2], Assael [3] and many other researchers [4, 5]. Hwang et al. [6] prepared four kinds of  
54 nanofluids using MWCNTs, CuO and SiO<sub>2</sub> nanoparticles. They found that the thermal  
55 conductivity of nanofluids was higher than its base fluid and the thermal conductivity of  
56 MWCNTs nanofluid was the highest than other nanofluids under the same concentration.

57 As a new research frontier, nanofluids two phase flow and thermal physics is the subject of  
58 growing concern [7, 8]. Investigation into the nanofluids phase change phenomena and  
59 complicated heat transfer mechanisms have intensively been performed over the past decade.  
60 Most researchers have found that the mechanisms of pool boiling heat transfer of nanofluids are  
61 different from those of conductive and convective heat transfer of nanofluids [11-13]. Yang and  
62 Maa [14] are possibly the first to conduct pool boiling experiments using nanofluids. Their  
63 experimental results have indicated that low concentrations of Al<sub>2</sub>O<sub>3</sub> nanofluids with 50 nm  
64 diameter can enhance the nucleate pool boiling heat transfer. Xue et al. [15] studied the boiling  
65 curve, bubble pattern and contact angle of gum acacia (GA) solution and carbon nanotubes  
66 nanofluids. The results showed GA solution enhanced transition boiling heat transfer rate, since  
67 GA powder improved the wettability of water. In addition, the critical heat flux of nanofluids  
68 pronouncedly increases than that of GA solution due to the deposition of nanoparticles. Amiri et  
69 al. [16] performed some pool boiling experiments using carbon nanotubes nanofluid considering  
70 different functional groups of nanotubes. They investigated the pool boiling HTC of covalent  
71 nanofluids increases than that of deionized water, the heat transfer of non-covalent nanofluids  
72 became worse for the reason of the effect of heat resistance. Sarafraz et al. [17-19] study the pool  
73 boiling of the MWCNTs and Al<sub>2</sub>O<sub>3</sub> nanofluids on several surfaces and conditions. About  
74 MWCNTs nanofluids, they found that the nucleate boiling of the nanofluids could still lead to

75 the particle deposition, but the micro-finned surfaces broke the deposition to enhance the  
76 nucleation site and thus the boiling heat transfer increasing. Shoghl et al. [20] studied the pool  
77 boiling heat transfer of nanofluids with ZnO,  $\alpha$ -Al<sub>2</sub>O<sub>3</sub> and MWCNTs. Their results indicate that  
78 the effects of boiling surface and properties of nanofluids to prove both of them may  
79 significantly influence the boiling heat transfer characteristics. For instance, the carbon  
80 nanotube-water nanofluids which improved the property of fluids and boiling surface  
81 characteristics could enhance the nucleate boiling heat transfer. Quite different results of nucleate  
82 boiling heat transfer with various surface conditions have been reported by researchers.  
83 Therefore, it is essential to explore and understand the various mechanisms governing the heat  
84 transfer processes.

85 According to the foregoing literature review, it is obvious that quite different results of  
86 boiling heat transfer with nanofluids and experimental conditions have been obtained. As pointed  
87 out by Cheng and Liu [7], there are still challenges to understand the boiling phenomena of  
88 nanofluids and their heat transfer mechanisms. Great effort should be made to achieve the  
89 complete and systematic knowledge in this aspect. In particular, it's still necessary to investigate  
90 and understand the heat transfer mechanisms through well designed and careful performed  
91 experiments and theoretical analysis.

92 Furthermore, the confined heat sink can be traced back to the ribbed radiator of CPU etc. In  
93 order to reduce the space and improve the heat efficiency of heat exchanger, flat plate heat pipe  
94 thermal spreader replaces the traditional radiator. The boiling in confined space condition just  
95 happens in this kind of heat pipe. Rops et al. [21] analyzed the nucleate boiling heat transfer on a  
96 spatially confined surface. They found that the depth of the boiling pot, the material of the  
97 bounding wall and the diameter of the inlet water supply didn't affect the enhancement of boiling  
98 heat transfer. Zhang et al. [22] reported an experimental investigation of phase-change  
99 phenomena in a small confined space. In the study, the boiling and condensation possessed

100 dramatically impacted each other and the bubbles were limited not only by the distance between  
101 boiling and condensation surface, but also by the condensation process. Liu and Yang [23]  
102 observed that the boiling heat transfer characteristics were affected by lots of factor in confined  
103 space, especially vapor blowing, liquid suction and vapor waving resistance. They also found the  
104 enhancement ratio of heat transfer coefficient reduced by the condition of decreasing boiling  
105 space or increasing heat flux. However, the study of boiling heat transfer using nanofluids in  
106 confined spaces at sub-atmospheric pressures is very limited in the literature so far. **Using  
107 nanofluid as working fluid seems a promising method of improving the heat transfer  
108 performance. The study on the mechanism of boiling heat transfer in confined with nanofluids is  
109 helpful to the application of nanofluids.** Therefore, it is necessary to conduct the relevant study in  
110 this aspect.

111 The objectives of this paper are to experimentally investigate the complicated nucleate  
112 boiling mechanisms of nanofluids in a confined space under a sub-atmospheric pressure  
113 condition. First, the technology used for preparation of nanofluids is described. Then,  
114 experiments of nucleate boiling heat transfer of the MWCNTs nanofluids were conducted in a  
115 confined space at a pressure of  $1 \times 10^{-3}$  Pa. The influences of heat flux, the concentration of  
116 nanofluids and surfactant on the heat transfer behaviors were presented. The scanning electron  
117 microscopy (SEM) photographs of boiling surfaces were used to analyze the modification by the  
118 deposition of nanoparticles. The roughness and contact angle of boiling surface and the  
119 visualization of the bubble behaviors were used to explain the boiling heat transfer mechanisms  
120 of the MWCNTs nanofluids.

## 121 **2. Technology of the water-based MWCNTs nanofluid preparation**

### 122 2.1. Characterization of the MWCNTs

123 The multi-walled carbon nanotube nanoparticles were manufactured by Beijing DK Nano

124 technology Co. Ltd utilizing the chemical vapor deposition method. The physical parameters of  
125 the MWCNTs are shown in Table 1. The MWCNTs have an outer diameter of 10-20 nm and an  
126 inner diameter of 5-10 nm. Their length is from 10 to 30  $\mu\text{m}$ . The density of the MWCNTs is 2.1  
127  $\text{g}/\text{cm}^3$  and its specific surface area is 200  $\text{m}^2/\text{g}$ . The purity of the MWCNTs is larger than 98%.  
128 Figure 1(a) shows a transmission electron microscopy (TEM) photograph of the multiple carbon  
129 walls of a tubular structure of the MWCNTs at a scale of 20 nm. Figure 1(b) shows a SEM  
130 photograph of the MWCNTs at scale of 500 nm. It can be seen that the nanoparticles  
131 agglomerate and twine together. Therefore, it is necessary to scatter the nanoparticles using  
132 physical and chemical methods [24-26] at first when preparing the water-based MWCNTs  
133 nanofluids.

## 134 2.2. Technology for preparation of the water-based MWCNTs nanofluid

135 In this study, magnetic stirrer and ultrasonic oscillation were adopted to disperse the  
136 MWCNTs in the base fluid deionized water. In addition, some surfactants were added in the base  
137 fluid to prevent the second aggregation and suspend the MWCNTs stably for a long time. In  
138 general, one step method or two step method is used for the preparation of the nanofluids [27].  
139 The two steps method was adopted to prepare the water-based MWCNTs nanofluids. The first  
140 step is to prepare the nanoparticles which have been manufactured. The surfactant is added into  
141 the base fluid and the solution is well mixed by stirring the solution with a magnetic stirrer for 5  
142 minutes. Then the nanoparticles are added into the surfactant solution. After 5 minutes stirring  
143 with the magnetic stirrer, the nanofluid is then well mixed with an ultrasonic oscillation for 1  
144 hour.

145 Selection of a surfactant was performed at first. Four different popular surfactants which  
146 have been used in the nanofluids preparation including cetyltrimethyl ammonium bromide  
147 (CTAB), polyvinyl pyrrolidone (PVP), sodium dodecyl benzene sulfonate (SDBS) and gum  
148 acacia (GA) were initially used in preparing the MWCNTs nanofluids. **The surfactants were all**

149 white particles and manufactured by Tianjin Fuchen Chemical Reagents Factory. The effects of  
150 surfactant on the stability of the nanofluids stability were studied through the static precipitation  
151 method. All the fresh prepared nanofluid samples with 0.1% volume concentrations of MWCNTs  
152 and four kinds of surfactants with 0.1% mass concentration looked similar in appearance, as  
153 shown in Fig. 2 (a). As is shown, the nanofluid with CTAB has foam at the liquid surface and the  
154 foam remains there for a long time. Foaming was found in the nanofluids with SDBS when  
155 prepared it, but it vanished quickly after standing a while. The nonion surfactants (PVP and GA)  
156 did not provide any foam. After standing for three months as shown in Fig. 2 (b), some obvious  
157 nanoparticles precipitation can be found in the nanofluids with the cation and anion surfactants  
158 (CTAB and SDBS). The nanofluids with the nonion surfactants have much better stability than  
159 cation and anion surfactants. Yazid et al. [28] pointed out that GA was frequently used as the  
160 surfactant to stabilize the carbon nanotubes in water. Our observation has confirmed their  
161 statement. Therefore, GA was chosen as the surfactant in preparing the water-based MWCNTs  
162 nanofluid used in the boiling experiments.

163 As mentioned above, stable dispersed nanofluids can be prepared adding GA with 0.1%  
164 mass concentration. Increasing the concentration of surfactant can explore the influence of the  
165 surfactant on boiling, so GA with four different mass concentrations of 0.1%, 0.3%, 0.5% and  
166 0.7% was respectively dissolved in the base fluids. The MWCNTs of five different volume  
167 fractions of 0.005%, 0.01%, 0.05%, 0.1% and 0.2% were added into the base fluids with or  
168 without the surfactant. All the MWCNTs nanofluids with and without GA were prepared for the  
169 boiling experiments in the present study.

### 170 3. Experimental setup and experiment procedure

171 The experimental setup consists of an experimental rig, an assembled test section and a  
172 measurement system. The details of these are elaborated here in this section.



### 173 3.1 . Experimental rig

174 Figure 3 shows the schematic diagram of the experimental rig used for the nucleate boiling  
175 heat transfer experiments in a confined space. The experimental rig mainly includes a  
176 thermostatic water container (1), voltage regulator (2), cartridge heaters (3), a copper rod (4),  
177 insulation layer (5), a copper sheet (6), quartz window (7), pressure gauge (8), a vacuum pump  
178 (9), a high-speed video camera (10), a data acquisition instrument (11) and a PC (12). It consists  
179 of a boiling system, a condensation system, a visualization quartz window together with a  
180 high-speed video camera, a measurement system and a PC for storing the measured parameters.

181 **The boiling system includes a test section, a copper rod, several cartridge heaters and a**  
182 **voltage regulator.** Four cartridge heaters were assembled inside a copper rod which is tightly  
183 contacted with a flat test section. The cartridge heaters connected to a voltage regulator are used  
184 to generate heat through electrical resistance and transfer the heat through the copper rod to the  
185 test section to generate boiling processes. The voltage regulator is used to adjust the heat flux in  
186 the boiling experiments.

187 The condensation system comprises a condensation chamber, a copper sheet and a  
188 thermostatic water container. Water in the thermostatic container was maintained at a constant  
189 temperature of 12°C and used to condensate the vapor generated in the test chamber. The  
190 vacuum device is used to remove the gas in the boiling test chamber before fill up the working  
191 fluid and maintain a sub-atmospheric pressure condition specified in the boiling experiments.  
192 The chamber wall between two copper sheets is made of a quartz window which is used for the  
193 visualization of the boiling process using the high-speed video camera.

194 Three **T type** thermocouples arranged along the axial direction of the copper rod are used to  
195 measure the local temperatures along the axis of the round copper rod. With the measured  
196 temperatures, the boiling surface temperature of the test section and heat flux can be calculated  
197 using one-dimensional linear heat conduction. The surface of the copper sheet was polished with

198 a 5000# sandpaper before the experiments. The data acquisition system is used to collect the  
199 temperatures of three points on the top of the copper heater, the fluid temperature, the vapor  
200 temperature in the test chamber and the operation pressure.

### 201 3.2 . Test section

202 Figure 4 shows the schematic diagram of the test section and the heating system. The  
203 heating section is mainly composed of the copper sheet, the copper rod and four cartridge heaters  
204 with a diameter of 8 mm. As is showed in Fig. 4, both sections of the upper and lower copper rod  
205 are cylindrical and four cartridge heaters are symmetrically arranged at the lower end of the rod  
206 to provide heat source for the boiling experiments. **The maximum heat flux was adjusted to 750**  
207 **kW/m<sup>2</sup> which does not reach critical heat flux as we focused on nucleate boiling heat transfer and**  
208 **mechanisms in our study.** The diameter of the upper copper rod is 20 mm, which has the same as  
209 the diameter of the boiling surface. Three **T type** thermocouples are arranged along the axis of  
210 the copper rod in the upper section of it to measure the local temperatures and then they are used  
211 to calculate the heat flux and the temperature of boiling surface in the boiling experiments.  
212 **Thermal grease was used to connect the thermocouples and copper rod, so the contact resistance**  
213 **could be neglected.** In order to investigate the boiling heat transfer characteristics of the  
214 MWCNTs nanofluids at sub-atmospheric pressure, the vacuum system is used to achieve the  
215 desired test pressure of  $1 \times 10^{-3}$  Pa. The top surface of the copper rod connected to a horizontal  
216 copper sheet which a thickness of only 0.3 mm. The thin sheet of copper has an excellent sealing  
217 effect while can neglect horizontal heat conduction effectively because of its thin axial size.

### 218 3.3 . Experimental procedure

219 To conduct the boiling experiments, first, the vacuum system was run for more than 30  
220 minutes to make the test chamber at a sub-atmospheric condition. Second, the working fluid was  
221 pumped into the test chamber. Following this, the vacuum device was operated again to  
222 discharge the dissolved gas escaped from the working fluid and an operation pressure of  $1 \times 10^{-3}$

223 Pa was maintained in the test chamber for the boiling experiments. Finally, the condensation  
224 system, the circulating water system, the data acquisition system and the power supply was  
225 started in sequence. The voltage regulator was used to adjust the voltage at several values of 50 V,  
226 70 V, 90 V, 100 V, 110 V, 120 V, and 130 V to generate different heat fluxes used for the test runs  
227 in the boiling experiments. After steady state was achieved for each test run, the measured  
228 parameters were taken by the data acquisition system and stored in the PC for further data  
229 reduction and analysis.

#### 230 4. Data reduction methods and uncertainty analysis

##### 231 4.1. Data reduction methods

232 With the measured parameters of local temperatures in the copper rod and the fluid  
233 temperature, the heat flux and boiling heat transfer coefficient may be calculated. The boiling  
234 heat transfer coefficient is calculated as:

$$235 \quad \quad \quad 236 \quad \quad \quad h = \frac{q}{T_w - T_f} \quad (1)$$

237 where  $T_w$  is the wall surface temperature of the test section and  $T_f$  is the saturation temperature  
238 of the working fluid,  $(T_w - T_f)$  is the superheat degree and  $q$  is the heat flux.

239 **It's not accurate to calculated heat flow by the voltage and current of the power supply due**  
240 **to a small amount of heat loss. Therefore,** the heat flux would be obtained through steady state  
241 heat conduction along the axial direction of the copper rod, assuming one dimensional heat  
242 conduction, as

$$243 \quad \quad \quad q = -\lambda \frac{dT}{dz} = -\lambda \cdot \frac{1}{2} \cdot \left( \frac{T_3 - T_2}{\Delta z_{3-2}} + \frac{T_2 - T_1}{\Delta z_{2-1}} \right) \quad (2)$$

244 where  $\lambda$  is the thermal conductivity of the copper heater,  $dT/dz$  is the average temperature  
245 gradient calculated according to the measured temperatures  $T_1$ ,  $T_2$ , and  $T_3$  as indicated in Fig. 4,  $z$

246 is the axial distance between the two temperature measurement points. **The calculated value of**  
 247 **heat flux is slightly lower than the power supply within 7%.**

248 The boiling surface temperature of the test section  $T_w$  is determined using one dimensional  
 249 conduction heat transfer along the vertical direction of the copper heater as:

$$250 \quad T_w = T_1 + \frac{dT}{dz} \Delta z_{w-1} = T_1 + \frac{1}{2} \times \left( \frac{T_3 - T_2}{\Delta z_{3-2}} + \frac{T_2 - T_1}{\Delta z_{2-1}} \right) \times 0.023 \quad (3)$$

251 To evaluate the enhancement of the nucleate boiling heat transfer of the nanofluids, the heat  
 252 transfer coefficient enhancement ratio is defined as:

$$253 \quad \eta = \frac{h_{nf} - h_{dw}}{h_{dw}} \times 100\% \quad (4)$$

254 where  $h_{nf}$  and  $h_{dw}$  are the boiling heat transfer coefficients of the MWCNTs nanofluids and the  
 255 deionized water respectively.

#### 256 4.2. Uncertainty analysis

257 The thermocouples were well calibrated before the experiments and the measured  
 258 temperatures are accurate to  $\pm 0.1$  K. The measured pressure gauge is accurate to 0.25% and the  
 259 distances between the two temperature measurement points are accurate to  $\pm 0.1$  mm. **The**  
 260 **accuracies of voltmeter and ammeter are  $\pm 0.1V$  and  $\pm 0.025A$ .**

261 **Using the methods of Kline and McClintock [29],** the uncertainties of heat flux and heat  
 262 transfer coefficient determined by Eqs. (1) and (2) may be analyzed as follows:

$$263 \quad \frac{\Delta q}{q} = \sqrt{\left( \frac{\Delta \lambda}{\lambda} \right)^2 + \left( \frac{\Delta \delta T}{\delta T} \right)^2 + \left( \frac{\Delta \delta z}{\delta z} \right)^2} \quad (5)$$

$$264 \quad \frac{\Delta h}{h} = \sqrt{\left( \frac{\delta q}{q} \right)^2 + \left( \frac{\Delta \delta T}{\delta T} \right)^2} \quad (6)$$

265 The uncertainly of thermal conductivity could be negligible, because the heater is processed  
 266 by a piece of standard copper. **Table 2 summaries the measurement uncertainties.** The uncertainty

267 of the heat flux is 2.02% and the uncertainty of heat transfer coefficient is 2.78%.

## 268 5. Experimental result and discussion

### 269 5.1 . Boiling heat transfer behaviours of the MWCNTs nanofluid and the deionized water

270 In order to compare the boiling heat transfer behaviors of the MWCNTs nanofluids to those  
271 of the deionized water, experiments of the test fluids were respectively run from single-phase  
272 heat transfer to the nucleate boiling under a sub-atmospheric pressure of  $1 \times 10^{-3}$  Pa.

273 Figure 5(a) shows the instantaneous variation of the boiling surface temperature with the  
274 heating time for both the nanofluids with the volume concentration of 0.05% and the base fluid  
275 at the heat flux of  $740 \text{ kW/m}^2$ . Figure 5(b) shows the variation of the heat transfer coefficient  
276 with the heating time. At the same heat flux, the boiling curve of the MWCNTs nanofluid is  
277 similar to that the base fluid. It can be seen that the boiling surface temperatures of both fluids  
278 reduce immediately at the boiling incipience. In the meantime, the heat transfer coefficients  
279 increase rapidly after the boiling incipience for both fluids. The boiling heat transfer coefficients  
280 gradually increase until reaching the steady state of boiling heat transfer. However, there are  
281 some differences boiling behaviors between the MWCNTs nanofluid and the base fluid water.  
282 On the one hand, the initial boiling surface temperature of the nanofluids is slightly lower than  
283 that of water. It indicates that the boiling incipience of the nanofluids occurs earlier than that of  
284 water. On the other hand, the boiling surface temperatures of the nanofluids are much lower than  
285 those of water and the transient boiling heat transfer coefficients of the nanofluids are much  
286 greater than those of water after reaching steady state boiling.

287 Figure 6(a) shows the photo of the MWCNTs deposition on the boiling surface. It shows  
288 that the nanoparticles are only adhered on the center of copper sheet although the all test section  
289 is uniform smooth copper surface. **It can be explained by the following reason: nanofluids are**  
290 **composed of solid phase of the nanoparticles and liquid phase of the deionized water. The phase**

291 change of nanofluids is generated on the boiling surface, and the liquid phase is vaporized and  
292 divorced from the surface. However, most of the nanoparticles cannot be taken away by the  
293 vapor. Therefore, the solid phase is separated from the liquid phase, so the nanoparticles stay on  
294 the boiling surface to form agglomerates and gradually produce a deposition. Thus, more and  
295 more nanoparticles are deposited on the boiling surface where the center of the copper sheet is.

296 The result of microscopic photograph by  $\times 80$  SEM in Fig. 6(b) shows the rough surface of  
297 deposition with pits and bulges. Fig. 6(c) by  $\times 30k$  SEM proves the point that the deposition is  
298 formed by irregular agglomeration of nanotube particles. The surface roughnesses of a copper  
299 surface polished by 5000# sandpaper and a nanoparticles surface by 0.05% volume fraction  
300 nanofluids deposition were tested using stylus profiler (DektakXT, Bruker, Germany). The  
301 copper surface roughness is 20.79 nm and the deposition surface is 4.82  $\mu\text{m}$ . Therefore, the  
302 deposition evidently changes the surface roughness of the test section and enhances the boiling  
303 heat transfer. This observation agrees to the experimental results by Kole and Dey [30]. They  
304 indicated that the surface roughness was influenced by deposition of the nanoparticles.

305 A static contact angle experiment using deionized water on the smooth surface and the  
306 deposition surface was measured by contact angle testing system (OCA15EC, Dataphysics,  
307 Germany). As is showed in Fig. 7, the nanoparticles deposition surface decrease 16 degree  
308 compared with the copper surface. The variation of contact angle has a great influence on the  
309 solid-liquid-vapor interface. Das et al. [31] pointed out that functionalized surface could reduce the  
310 contact angle to enhance boiling heat transfer. The MWCNTs deposition is conducive to wet the  
311 surface, make bubbles easier departure from the boiling surface and increase the boiling heat  
312 transfer coefficient. Overall, the main reason of enhanced boiling heat transfer is due to the  
313 deposition of agglomerate nanoparticles which may increase the nucleate sites and bubble  
314 frequency.

315 5.2 . The effects of the MWCNTs concentrations and the surfactant on the nucleate boiling heat  
316 transfer behaviours

317 Experiments of the boiling heat transfer characteristics of the MWCNTs nanofluid with  
318 different volume concentrations from 0.005% to 0.2% without surfactant were conducted at a  
319 sub-atmospheric pressure of  $1 \times 10^{-3}$  Pa. First, experiments were conducted at a heat flux of 100  
320  $\text{kW/m}^2$  at which the first bubble would generate for the boiling of the deionized water as  
321 observed via visualization. Figure 8(a) shows the variation of heat flux versus the superheat  
322 degree for the boiling processes with the MWCNTs nanofluid with three volume concentrations  
323 of 0.005%, 0.01% and 0.05% and the deionized water at the steady state test conditions. Figure  
324 8(b) shows the variation of boiling heat transfer coefficient versus the heat flux for the  
325 corresponding test fluids respectively. The experimental results demonstrate that the nanofluids  
326 lead to reducing the boiling surface temperatures compared to those of water under the same heat  
327 flux. This means that addition of the MWCNTs in the deionized water can enhance the boiling  
328 heat transfer. As shown in Fig. 8(b), the heat flux has a significant effect on the boiling heat  
329 transfer coefficient. The boiling heat transfer coefficient increases with increasing the heat flux  
330 for both the nanofluids and the base fluid. Furthermore, the boiling heat transfer coefficient of  
331 the base fluid can be enhanced by adding the MWCNTs in view of boiling curves shifting to the  
332 left. It is obvious as indicated that increasing the concentration of the MWCNTs nanofluid may  
333 lead to an enhancement of boiling heat transfer. The enhancement increases with increasing the  
334 concentration in the present study. The main reason is that increasing concentration of the  
335 nanofluid increases the deposition of the nanoparticles on the boiling heat transfer surface and  
336 thus increases the nucleation sites and bubble frequency, as such more bubbles may be generated  
337 in the boiling process.

338 Figure 9 shows the comparison of the boiling heat transfer coefficient with the MWCNTs  
339 volume concentration at a lower heat flux of  $100 \text{ kW/m}^2$  and a higher heat flux of  $740 \text{ kW/m}^2$ .

340 The heat transfer coefficients at the higher heat flux are around 4 times higher than those at the  
341 lower heat flux. The heat transfer coefficient is enhanced with increasing the concentration,  
342 although the particle deposition may cause some thermal resistance. Therefore, the thickness of  
343 deposition would not be the major factor of HTC in this study. It should be noted that there is a  
344 fast-increasing of the nucleate boiling heat transfer coefficients occurred at lower concentrations  
345 of the nanofluids. However, this variation of the boiling heat transfer coefficients becomes flat at  
346 higher concentrations. It means that this is a critical concentration of the nanofluid at which the  
347 boiling heat transfer enhancement remains unchanged beyond this critical concentration. This  
348 effect of the nanofluids concentration on the boiling heat transfer coefficient enhancement may  
349 be attributed to the variation of the surface roughness due to the nanoparticles deposition.  
350 However, there is no significant change with further increasing the concentration of the  
351 nanofluid beyond the critical concentration and thus the enhancement of the boiling heat transfer  
352 coefficient remains unchanged.

353 Addition of a surfactant has an important influence on the physical properties of nanofluid  
354 such as the surface tension, viscosity, thermal conductivity [32, 33] and the nucleate boiling heat  
355 transfer behaviors [34, 35]. In order to understand the effects of various surfactants on the  
356 boiling heat transfer behavior in the present study, four different mass concentrations of GA  
357 (0.1%, 0.3%, 0.5%, 0.7%) were added into the nanofluid of 0.1% volume concentration of  
358 MWCNTs. Figure 10 shows the variation of the boiling heat transfer coefficient with the mass  
359 concentration of GA at three different heat fluxes of 520, 630 and 740 kW/m<sup>2</sup>. It is obvious that  
360 the variations of the heat transfer coefficients clearly indicate that the boiling heat transfer is  
361 deteriorated with increasing the concentration of GA in the nanofluids. Furthermore, the heat  
362 transfer coefficient curves fall down sharply with increasing the heat flux. It means the negative  
363 effect of surfactant GA on the boiling heat transfer becomes more significant at a higher heat flux  
364 than those at a lower heat flux.



365 The conditions of the nanofluids before and after the boiling processes were compared with  
366 each other as to understand how the boiling process affects the nanofluid. Figure 11 shows the  
367 photographs of the MWCNTs nanofluid before and after boiling processes. Figure 11(a) shows  
368 the condition of the prepared nanofluids in all concentrations of GA. The nanofluid is black and  
369 the multi-walled carbon nanotube particles are well mixed in the base fluid after ultrasonic  
370 oscillation. Figure 11 (b) and (c) shows the condition of the MWCNTs nanofluid after boiling  
371 without and with surfactant GA, respectively. The MWCNTs in nanofluid without GA  
372 agglomerate and deposit at the bottom of nanofluid after boiling while the nanofluid with  
373 surfactant GA still keep good dispersion after boiling process. **With increasing heat flux, the  
374 activity of nanoparticles is more severe in the liquid, which is helpful to the dispersion of  
375 nanoparticles by surfactant. However, the main reason for the enhancement of heat transfer by  
376 nanofluid is the aggregation layer of the nanoparticles on the boiling surface. According to this  
377 observation, it is obvious that the surfactant can make particles uniformly dispersed in the base  
378 fluid and inhibit the deposition generated on the boiling surface, reduce the roughness of boiling  
379 surface and weaken the active nucleation sites.**

### 380 5.3 . The enhancement ratio of boiling heat transfer coefficients of the MWCNTs nanofluid

381 In order to evaluate the heat transfer enhancement performance, the boiling heat transfer  
382 coefficient enhancement ratios of the nanofluids with four different MWCNTs concentrations of  
383 0.005%, 0.01%, 0.05% and 0.1% are compared with each other here. Figure 12 shows the  
384 variation of the heat transfer coefficient enhancement ratio versus the heat flux from  $100 \text{ kW/m}^2$   
385 to  $740 \text{ kW/m}^2$ . The maximum heat transfer enhancement ratio is 40.53%. Furthermore, the heat  
386 transfer enhancement ratio initially decreases with increasing the heat flux until a value of about  
387  $340 \text{ kW/m}^2$  and then increases with increasing the heat flux after this initial decrease. The heat  
388 transfer enhancement ratio trends can be explained through the bubble formation and departure  
389 behaviors through the visualization of the boiling processes using a high-speed video camera.

390 In order to observe the variation of bubble formation clearly, boiling experiments of the  
391 deionized water were conducted on the surface with deposition. The MWCNTs nanofluid was  
392 replaced with the deionized water and the deposition of the MWCNTs was kept on the boiling  
393 surface, which was formed by nanofluid with 0.05% concentration after boiling. The bubble  
394 generation, growth and departure processes were observed to explain the experimental results  
395 and the heat transfer mechanisms.

396 Figure 13 shows the comparison of the bubble generation processes observed at a low heat  
397 flux of  $100 \text{ kW/m}^2$  and a high heat flux of  $740 \text{ kW/m}^2$  on the boiling surface with the deposition  
398 of the MWCNTs. As shown in Fig. 13(a), a bubble emerges on the boiling surface and kept  
399 growing. **At low pressure, the superheated liquid is full around the bubbles because of the low**  
400 **boiling point of working fluid. On the one hand, with the bubble rising, the bubble volume**  
401 **increases with the increase of the pressure. On the other hand, the bubble dramatically becomes**  
402 **large because the water around the bubble continually vaporizes into the bubble.** Shortly  
403 afterwards, it departs from the surface slowly which may deteriorate the heat transfer from the  
404 boiling surface to the fluid. **The vapor condenses rapidly after contacting the upper copper**  
405 **surface.** At last, the liquid back to initial state without phase-change.

406 As mentioned in the fore-going, the deposition of the nanoparticles on the boiling surface  
407 evidently improves the number of nucleation sites and **contact angle** which can increase and  
408 reduce the region of no phase-change. The slower generation and departure of bubble, the more  
409 obvious enhancement of heat transfer of deposition. **At lower heat flux, the increase of the**  
410 **bubble formation rate is the most important mechanism to enhanced heat transfer by nanofluids.**  
411 **But with increasing the heat flux, the bubble formation rate also increases, hence heat transfer**  
412 **enhancement of nanofluids with increasing heat flux becomes weak.** As observed in Fig. 12, this  
413 transitional heat flux is around  $340 \text{ kW/m}^2$  where the bubbles become continuous. Thus the  
414 boiling heat transfer coefficient enhancement ratios continue to decline from 100 to  $340 \text{ kW/m}^2$

415 heat fluxes.

416 The different boiling patterns at a higher heat flux are shown in Fig. 13(b). It shows that  
417 more than one bubble generated from the boiling surface and grew bigger rapidly, and then the  
418 bubbles departure becomes fast. New bubbles generated immediately when the previous bubbles  
419 just left and the heat transfer becomes stable. Shoghl et al. [20] proposed the effect of both  
420 deposition surface and properties of nanofluids influenced the boiling heat transfer coefficient.  
421 The enhanced heat transfer mechanisms at high heat fluxes are attributed to not only the increase  
422 of the nucleation site density but also the disturbance of particles in fluid. In this study, the  
423 experimental results also show that the enhancement ratio of boiling heat transfer coefficient can  
424 be increased by improving the effect of deposition and degree of particle disturbance with  
425 increasing heat flux at high heat fluxes from 340 to 740 kW/m<sup>2</sup>.

## 426 6. Conclusions

427 In the present study, first, stable and uniform nanofluid preparation technology is introduced.  
428 Then, experiments of nucleate boiling heat transfer characteristics of the MWCNT water-based  
429 nanofluids and the base fluid deionized water in a confined space were conducted at a  
430 sub-atmospheric pressure of  $1 \times 10^{-3}$  Pa and heat fluxes from 100 to 740 kW/m<sup>2</sup>. **The uncertainty  
431 of the heat flux is 2.02% and the uncertainty of heat transfer coefficient is 2.78%. The roughness  
432 and contact angle of the deposited layer and copper surface were compared.** The effects of the  
433 concentrations of nanoparticles and surfactants on the boiling heat transfer behaviors have been  
434 analyzed. The bubble generation and departure characteristics together with the observed particle  
435 deposition on the boiling heat transfer surface have been used to explain the experimental results  
436 and the heat transfer enhancement mechanisms. The effects of heat flux on the heat transfer  
437 enhancement have also been discussed. From the present study, the following conclusions have  
438 been reached:

- 439 (1) Stable and uniform water-based MWCNTs nanofluid can be produced using the two steps  
440 method with addition of GA.
- 441 (2) Compared with the base fluid, the MWCNTs nanofluid can enhance boiling heat transfer.  
442 The maximum heat transfer enhancement can reach 40.53%. The main reason of the heat  
443 transfer enhancement is due to the deposition of the MWCNTs on the boiling surface which  
444 can increase the roughness and reduce the contact angle.
- 445 (3) The boiling heat transfer coefficient increases with increasing concentration of the MWCNTs  
446 nanofluids owing to increasing nucleation sites of boiling surface and bubble formation rate.  
447 A critical volume concentration was found where the boiling heat transfer coefficient will not  
448 be further enhanced. In general, it is limited to enhance the boiling heat transfer coefficient  
449 by nanofluids because further deposition of the nanoparticles won't obviously improve the  
450 boiling surface.
- 451 (4) Addition a surfactant may keep the stable and uniform of the MWCNTs nanofluid. However,  
452 it seems that the surfactant has a negative effect on the boiling heat transfer in the present  
453 study. Addition of GA inhibits the formation of deposition and thus weakens the boiling heat  
454 transfer of the nanofluid. The higher the concentration of GA, the worse the boiling heat  
455 transfer is.
- 456 (5) The heat flux has a significant effect on the boiling heat transfer ratio. The boiling heat  
457 transfer enhancement ratio decreases with increasing the heat flux when the heat flux is less  
458 than  $340 \text{ W/m}^2$  while it increases with increasing the heat flux beyond this value.
- 459 (6) The mechanisms of the boiling heat transfer enhancement of the MWCNTs nanofluid are  
460 quite different for the lower and higher heat fluxes. At the low heat fluxes, the deposition  
461 layer increases the bubble formation frequency, and substantially strengthens the boiling heat  
462 transfer. At the high heat fluxes, the increase of nanoparticles concentration and heat flux  
463 enhances particle disturbance in fluid. Besides, with the enhancement of deposition and

464 particle disturbance, the enhancement ratio of boiling heat transfer coefficient is evidently  
465 increased.

466

## 467 **Acknowledgements**

468 This work is supported by a research fund of the National Natural Science Foundation of China (No.  
469 51576005).

470

## **References**

- [1] S.U.S. Choi, Enhancing thermal conductivity of fluids with nanoparticles, *Developments and Application of Non-newtonian Flows*, ASME 66 (1995) 99-105.
- [2] Y.M. Xuan, Q. Li, W.F. Hu, Aggregation structure and thermal conductivity of nanofluids, *AIChE J.* 49 (4) (2003) 1038-1043.
- [3] M.J. Assael, C.F. Chen, I. Metaxa, W.A. Wakeham, Thermal Conductivity of Suspensions of Carbon Nanotubes in Water, *Int. J. Thermophys.* 25 (4) (2004) 971-985.
- [4] S.A. Angayarkanni, J. Philip, Review on thermal properties of nanofluids: Recent developments, *Adv. Colloid Interface Sci.* 225 (2015) 146-176.
- [5] M. Raja, R. Vijayan, P. Dineshkumar, M. Venkatesan, Review on nanofluids characterization, heat transfer characteristics and applications, *Renew. Sust. Energ. Rev.* 64 (2006) 163-173.
- [6] Y.J. Hwang, Y.C. Ahn, H.S. Shin, C.G. Lee, G.T. Kim, H.S. Park, J.K. Lee, Investigation on characteristics of thermal conductivity enhancement of nanofluids, *Curr. Appl. Phys.* 6 (2006) 1068-1071.
- [7] L. Cheng, L. Liu, Boiling and two-phase flow phenomena of refrigerant-based nanofluids: Fundamentals, applications and challenges, *Int. J. Refrig.* 36 (2) (2013) 421-446.

- [8] L. Cheng, E.P. Bandarra Filho, J.R. Thome, Nanofluid two-phase flow and thermal physics: A new research frontier of nanotechnology and its challenges, *J. Nanosci. Nanotech.* 8 (2008) 3315-3332.
- [9] G.D. Xia, R. Liu, J. Wang, M. Du, The characteristics of convective heat transfer in microchannel heat sinks using  $\text{Al}_2\text{O}_3$  and  $\text{TiO}_2$  nanofluids, *Int. Commun. Heat Mass Transf.* 76 (2016) 256-264.
- [10] D. Yadav, J Wang, R Bhargava, J Lee, H.H. Cho, Numerical investigation of the effect of magnetic field on the onset of nanofluid convection, *Appl. Therm. Eng.* 103 (2016) 1441-1449.
- [11] D. Ciloglu, A. Bolukbasi, A comprehensive review on pool boiling of nanofluids, *Appl. Therm. Eng.* 84 (2015) 45-63.
- [12] R. Kamatchi, S. Venkatachalapathy, Parametric study of pool boiling heat transfer with nanofluids for the enhancement of critical heat flux: A review, *Int. J. Therm. Sci.* 87 (2015) 228-240.
- [13] X.D. Fang, Y.F. Chen, H.L. Zhang, W.W. Chen, A.Q. Dong, R. Wang, Heat transfer and critical heat flux of nanofluid boiling: A comprehensive review, *Renew. Sust. Energ. Rev.* 62 (2016) 924-940.
- [14] Y.M. Yang, J.R. Maa, Boiling of suspension of solid particles in water, *Int. J. Heat Mass Transf.* 27 (1984) 145-147.
- [15] H.S. Xue, J.R. Fan, R.H. Hong, Y.C. HU, Characteristic boiling curve of carbon nanotube nanofluid as determined by the transient calorimeter technique, *Appl. Phys. Lett.* 90 (90) (2007) 99-105.
- [16] A. Amiri, M. Shanbedi, H. Amiri, S. Zeinali Heris, S.N. Kazi, et al, Pool boiling heat transfer of CNT/water nanofluids, *Appl. Therm. Eng.* 71 (71) (2014) 450–459.
- [17] M.M. Sarafraz, F. Hormozi, Nucleate pool boiling heat transfer characteristics of dilute

- $\text{Al}_2\text{O}_3$ -ethyleneglycol nanofluids, *Int. Commun. Heat Mass Transf.* 58 (2014) 96-104.
- [18] M.M. Sarafraz, F. Hormozi, Experimental investigation on the pool boiling heat transfer to aqueous multi-walled carbon nanotube nanofluids on the micro-finned surfaces, *Int. J. Therm. Sci.* 100 (22) (2015) 255-266.
- [19] M.M. Sarafraz, F. Hormozi, S.M. Peyghambarzadeh, Pool boiling heat transfer to aqueous alumina nano-fluids on the plain and concentric circular micro-structured (CCM) surfaces, *Exp. Therm. Fluid Sci.* 72 (2016) 125-139.
- [20] S.N. Shoghl, M. Bahrami, M. Jamialahmadi, The Boiling Performance of  $\text{ZnO}$ ,  $\alpha\text{-Al}_2\text{O}_3$  and MWCNTs-Water Nanofluids: An Experimental Study, *Exp. Therm. Fluid Sci.* 80 (2016) 27-39.
- [21] C.M. Rops, R. Lindken, J.F.M. Velthuis, J. Westerweel, Enhanced heat transfer in confined pool boiling, *Int. J. Heat Fluid Flow* 30 (4) (2009) 751-760.
- [22] G.M. Zhang, Z.L. Liu, C. Wang, An experimental study of boiling and condensation co-existing phase change heat transfer in small confined space, *Int. J. Heat Mass Transf.* 64 (2) (2013) 1082-1090.
- [23] C.F. Liu, C.Y. Yang, Effect of space distance for boiling heat transfer on micro porous coated surface in confined space, *Exp. Therm. Fluid Sci.* 50 (10) (2013) 163-171.
- [24] A. Ghozatloo, A.M. Rashidi, M. Shariaty-Niasar, Effects of surface modification on the dispersion and thermal conductivity of CNT-water nanofluids, *Int. Commun. Heat Mass Transf.* 54 (46) (2014) 304-310.
- [25] M. Farbod, A. Ahangarpour, S.G. Etemad, Stability and thermal conductivity of water-based carbon nanotube nanofluids, *PARTICUOLOGY* 22 (5) (2015) 59-65.
- [26] W.S. Sarsam, A. Amiri, S.N. Kazi, A.Badarudin, Stability and thermophysical properties of non-covalently functionalized graphene nanoplatelets nanofluids, *Energy Convers. Manage.* 116 (2016) 101-111.

- [27] D.K. Devendira, V.A. Amirtham, A review on preparation, characterization, properties and applications of nanofluids, *Renew. Sust. Energ. Rev.* 60 (2016) 21-40.
- [28] M.N.A.W.M. Yazid, N.A.C. Sidik, R. Mamat, G. Najafi, A review of the impact of preparation on stability of carbon nanotube nanofluids, *Int. Commun. Heat Mass Transf.* 78 (2016) 253-263.
- [29] S.J. Kline, F.A. McClintock, Describing Uncertainties in Single-Sample Experiments, *Mech. Eng.* 75 (1) (1953) 3-8.
- [30] M. Kole, T.K. Dey, Investigations on the pool boiling heat transfer and critical heat flux of ZnO-ethylene glycol nanofluids, *Appl. Therm. Eng.* 37 (16) (2012) 112-119.
- [31] S. Das, B. Saha, S. Bhaumik, Experimental study of nucleate pool boiling heat transfer of water by surface functionalization with SiO<sub>2</sub> nanostructure, *Exp. Therm. Fluid Sci.* 81 (2016) 454-465.
- [32] M.Z. Zhou, G.D. Xia, J. Li, L. Chai, L.J. Zhou, Analysis of factors influencing thermal conductivity and viscosity in different kinds of surfactant solutions, *Exp. Therm. Fluid Sci.* 36 (2012) 22-29.
- [33] G.D. Xia, H.M. Jiang, R. Liu, Y.L. Zhai, Effects of surfactant on the stability and thermal conductivity of Al<sub>2</sub>O<sub>3</sub>-deionized water nanofluids, *Int. J. Therm. Sci.* 48 (2014) 118-124.
- [34] L. Cheng, D. Mewes, A. Luke, Boiling phenomena with surfactants and polymeric additives: A state-of-the-art review, *Int. J. Heat Mass Transf.* 50 (13-14) (2007) 2744-2771.
- [35] A. Najim, V. More, A. Thorat, S. Patil, S. Savale, Enhancement of pool boiling heat transfer using innovative non-ionic surfactant on a wire heater, *Exp. Therm. Fluid Sci.* 82 (2017) 375-380.



## Nomenclatures

h	heat transfer coefficient, W/ m <sup>2</sup> ·K
q	heat flux, W/m <sup>2</sup>
T	temperature, K
z	distance between two temperature measurement points, m

## Greek symbols

$\lambda$	thermal conductivity, W/ m·K
$\eta$	enhancement ratio of boiling heat transfer coefficient, %

## Subscripts

f	working fluid
w	boiling surface
nf	nanofluids
dw	deionized water

## Abbreviations

GA	gum acacia
MWCNTs	multi-walled carbon nanotubes
SEM	scanning electron microscopy
TEM	transmission electron microscopy

## List of Table and Figure Captions

**Table 1** Parameters of multi-walled carbon nanotube nanoparticles.

**Table 2** The summary of measurement uncertainties

**Fig. 1.** Microscopic photograph of the MWCNTs by (a) TEM and (b) SEM .

**Fig. 2.** The images of the dispersed MWCNTs nanofluids with four different surfactants: (a) Fresh prepared nanofluids and (b) Nanofluids after standing for three months.

**Fig. 3.** Schematic diagram of the experimental rig. (1) Thermostatic water container, (2) Voltage regulator, (3) Cartridge heater, (4) Copper rod, (5) Insulation layer, (6) Copper sheet, (7) Quartz window (8) Pressure gauge, (9) Vacuum pump, (10) High-speed camera, (11) Data acquisition instrument, (12) PC.

**Fig. 4.** Schematic diagram of the test section and the heating arrangement.

**Fig. 5.** Boiling curves of the MWCNTs nanofluid with a volume concentration of 0.05% and deionized water: (a) Boiling surface temperature vs. time; (b) Boiling heat transfer coefficient vs. time.

**Fig. 6.** Macroscopic and microscopic photographs of nanoparticles deposition: (a) by camera, (b) by  $\times 80$  SEM, (c) by  $\times 30k$  SEM.

**Fig. 7.** Static contact angle of (a) a smooth copper surface and (b) a nanoparticles deposition surface.

**Fig. 8.** Boiling curves of the MWCNTs nanofluids with three different volume concentrations of 0.005%, 0.01% and 0.05%, and the deionized water: (a) Heat flux vs. superheat degree, (b) Boiling heat transfer coefficient vs. heat flux.

**Fig. 9.** Variation of the boiling heat transfer coefficients of the MWCNTs nanofluids with the concentrations at two different heat fluxes of  $100 \text{ kW/m}^2$  and  $740 \text{ kW/m}^2$ .

**Fig. 10.** Variation of the boiling heat transfer coefficient with the mass concentration of surfactant GA at three different heat fluxes of  $520 \text{ kW/m}^2$ ,  $630 \text{ kW/m}^2$  and  $740 \text{ kW/m}^2$ .

**Fig. 11.** Agglomeration condition of the MWCNTs nanofluids: (a) before boiling, (b) without GA after boiling, (c) with GA after boiling.

**Fig. 12.** Variation of the boiling heat transfer coefficient enhancement ratios of the MWCNTs nanofluids with the heat flux for four different volume fractions of 0.005%, 0.01%, 0.05% and 0.1%.

**Fig. 13.** Photographs of the bubble generation, growth and departure on the boiling surface with the MWCNTs deposition at two heat fluxes: (a) 100kW/m<sup>2</sup> and (b) 740kW/m<sup>2</sup>.

**Table 1**

Parameters of the multi-walled carbon nanotube nanoparticles.

Outer diameter(nm)	Inner diameter(nm)	Length (μm)	Purity	Density (g/cm <sup>3</sup> )	Specific surface area(m <sup>2</sup> /g)
10-20	5-10	10-30	>98%	2.1	200



**Table 2**

The summary of measurement uncertainties.

Parameter	Unit	Uncertainty
Temperature	K	$\pm 0.1$
Distance between thermal couples	mm	$\pm 0.1$
Voltage	V	$\pm 0.1$
Current	A	$\pm 0.025$
Pressure	Pa	0.25%
Heat flux	W/m <sup>2</sup>	2.02%
Heat transfer coefficient	W/ m <sup>2</sup> ·K	2.78%

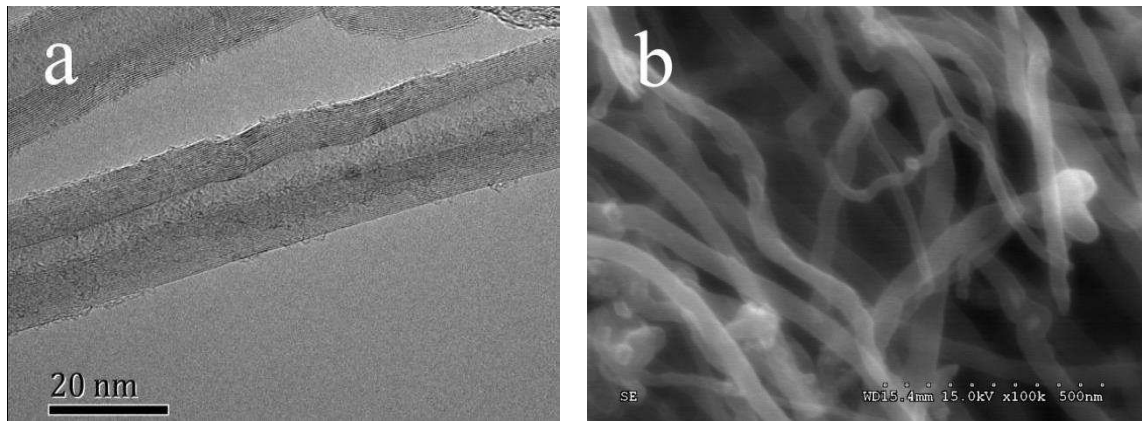
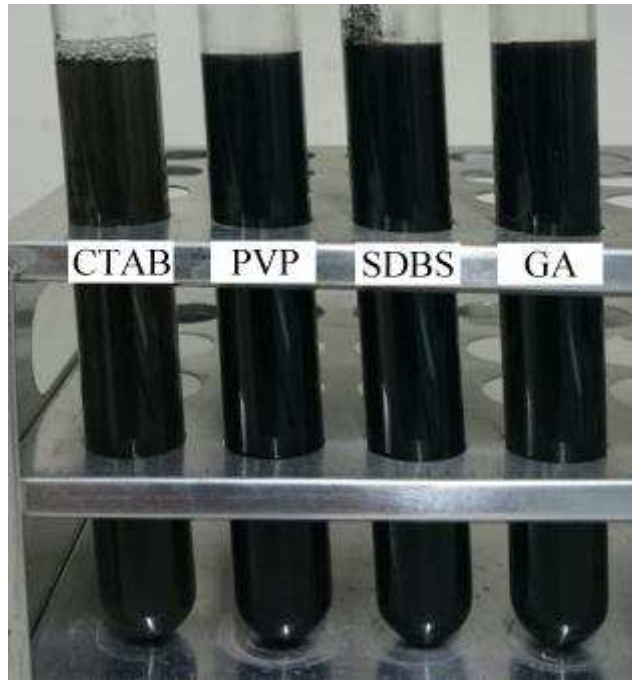
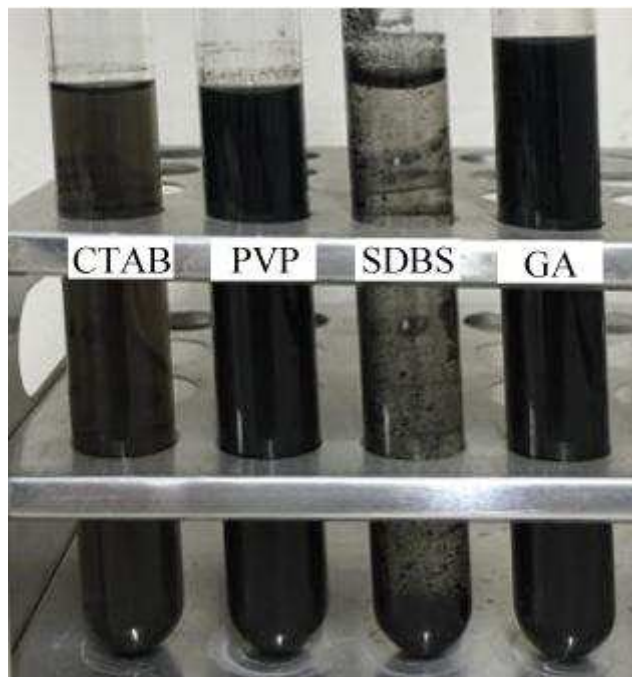


**Fig. 1.** Microscopic photograph of the MWCNTs by (a) TEM and (b) SEM .



(a) Fresh prepared nanofluids.



(b) Nanofluids after standing for three months.

**Fig. 2.** The images of the dispersed MWCNTs nanofluids with four different surfactants: (a) Fresh prepared nanofluids and (b) Nanofluids after standing for three months.

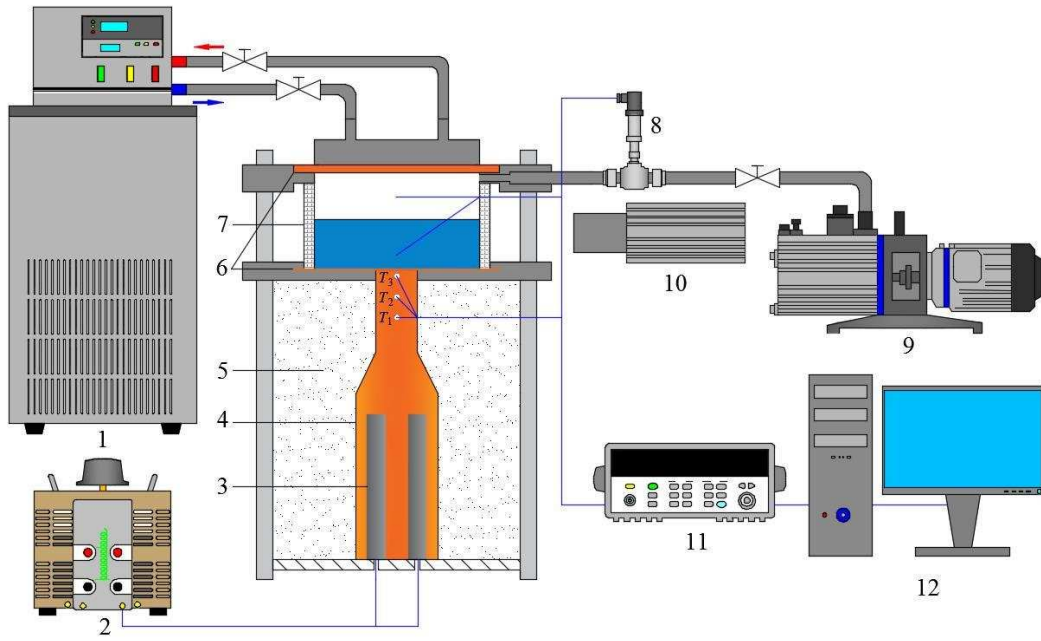


**Fig. 3.** Schematic diagram of the experimental rig.

- (1) Thermostatic water container, (2) Voltage regulator, (3) Cartridge heater, (4) Copper rod, (5) Insulation layer, (6) Copper sheet, (7) Quartz window (8) Pressure gauge, (9) Vacuum pump, (10) High-speed camera, (11) Data acquisition instrument, (12) PC.



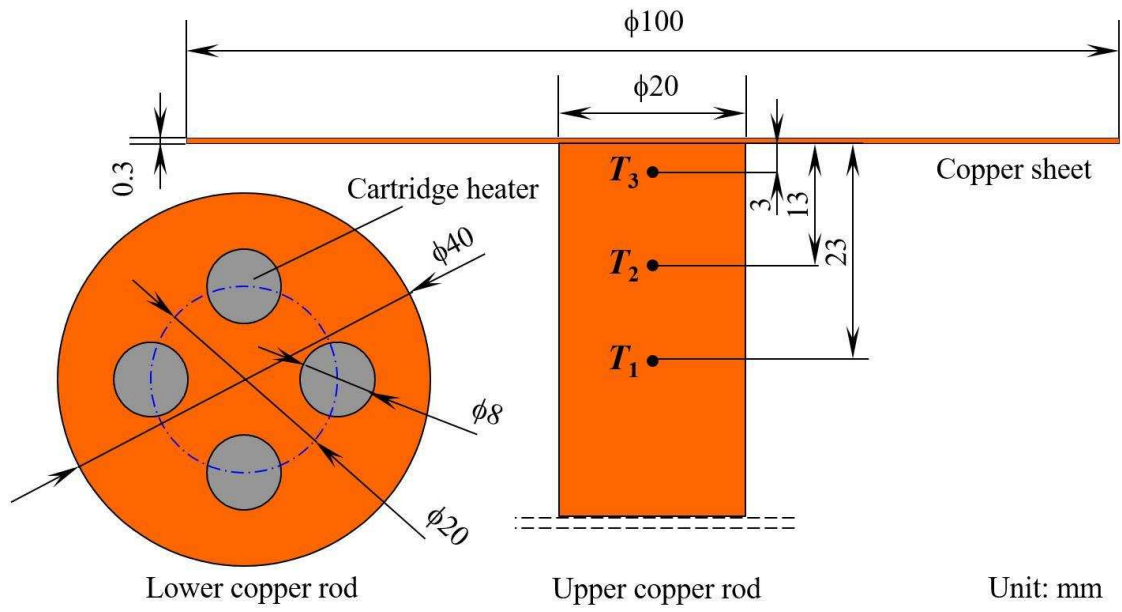


**Fig. 4.** Schematic diagram of the test section and the heating arrangement.

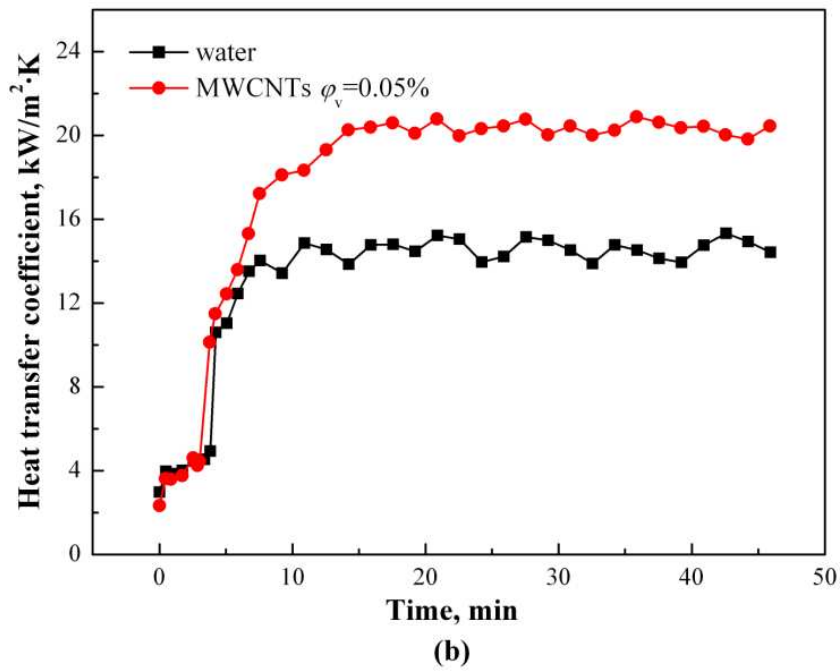
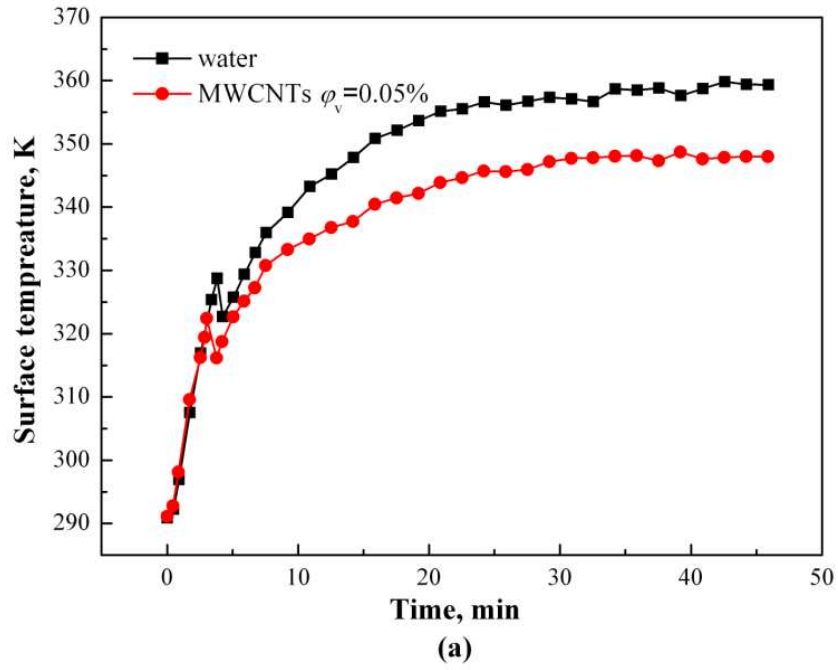


**Fig. 5.** Boiling curves of the MWCNTs nanofluid with a volume concentration of 0.05% and deionized water: (a) Boiling surface temperature vs. time; (b) Boiling heat transfer coefficient vs. time.

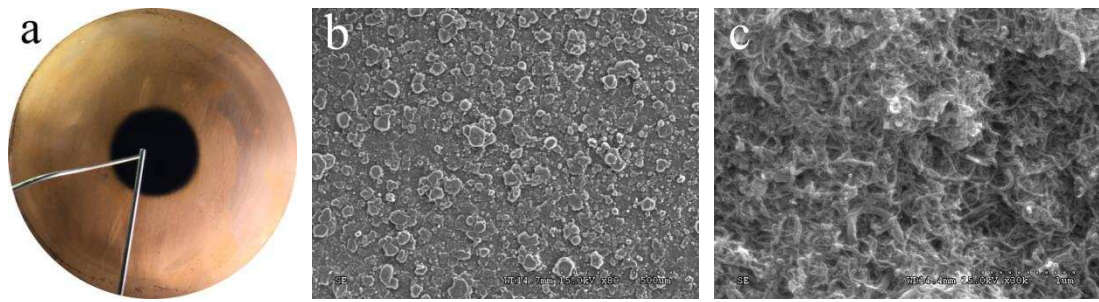


**Fig. 6.** Macroscopic and microscopic photographs of nanoparticles deposition: (a) by camera, (b) by  $\times 80$  SEM, (c) by  $\times 30k$  SEM.

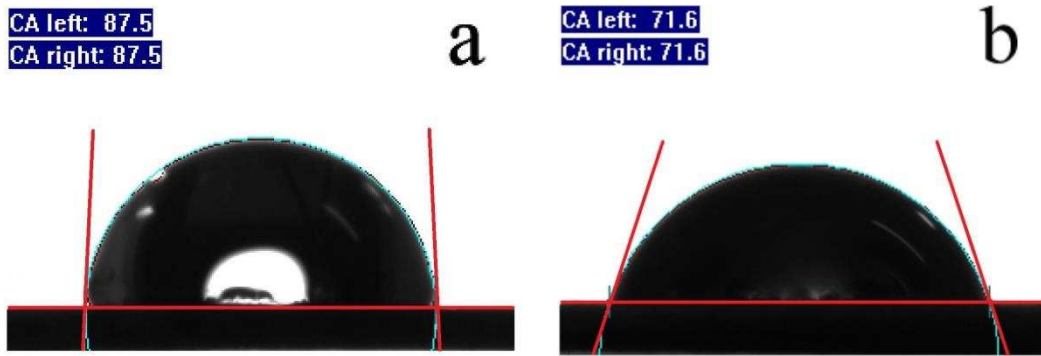


**Fig. 7.** Static contact angle of (a) a smooth copper surface and (b) a nanoparticles deposition surface.

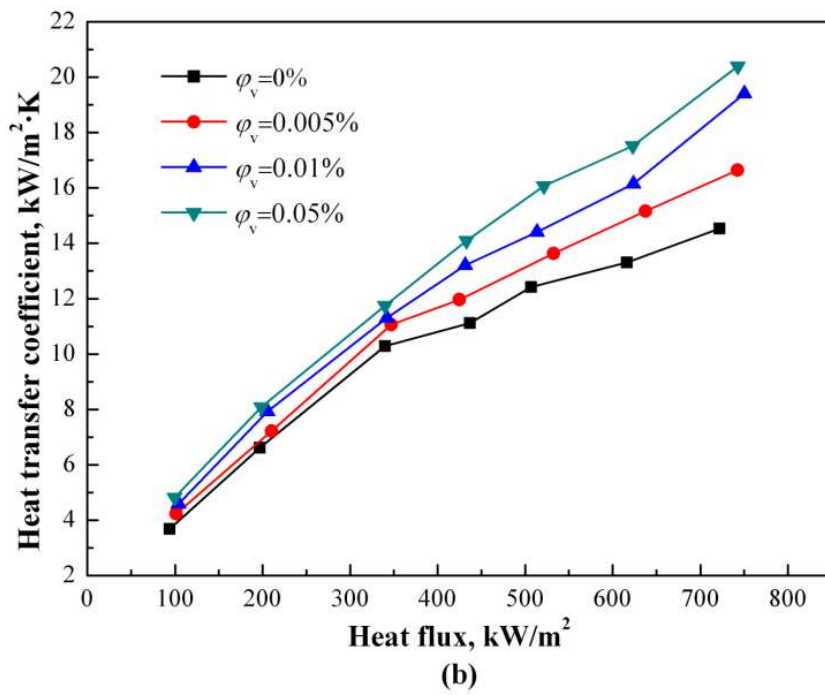
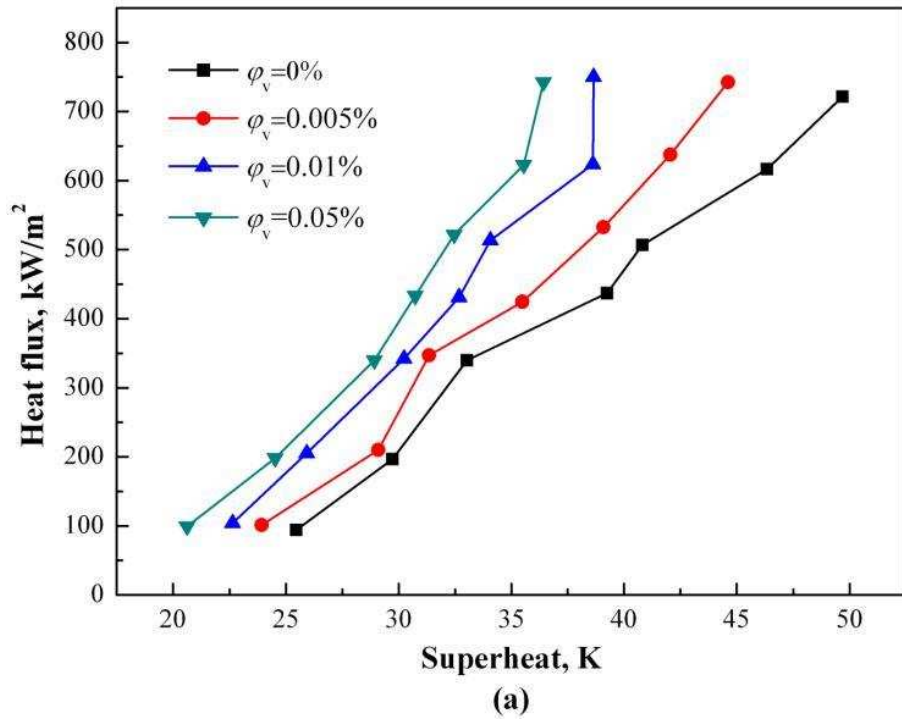


**Fig. 8.** Boiling curves of the MWCNTs nanofluids with three different volume concentrations of 0.005%, 0.01% and 0.05%, and the deionized water: (a) Heat flux vs. superheat degree, (b) Boiling heat transfer coefficient vs. heat flux.

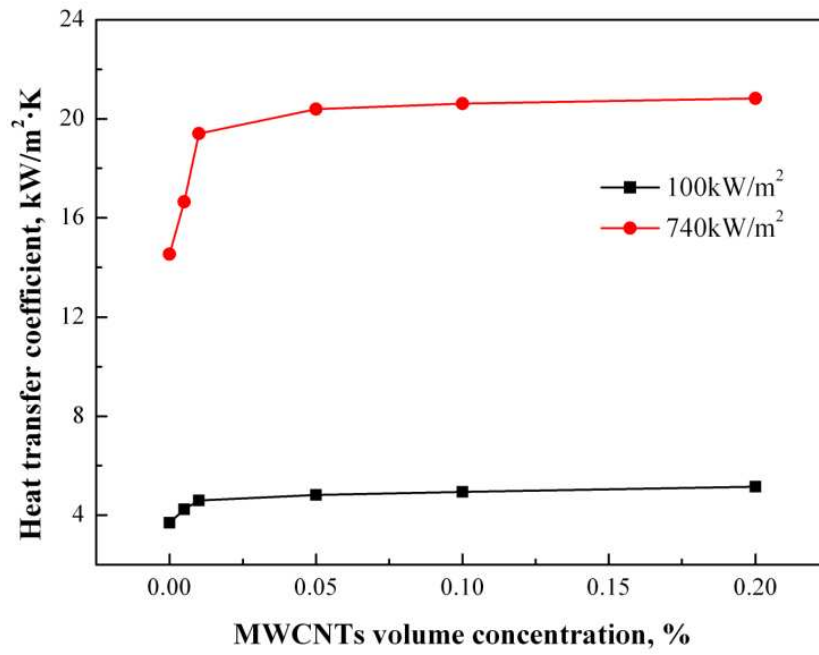


**Fig. 9.** Variation of the boiling heat transfer coefficients of the MWCNTs nanofluids with the concentrations at two different heat fluxes of 100 kW/m<sup>2</sup> and 740 kW/m<sup>2</sup>.

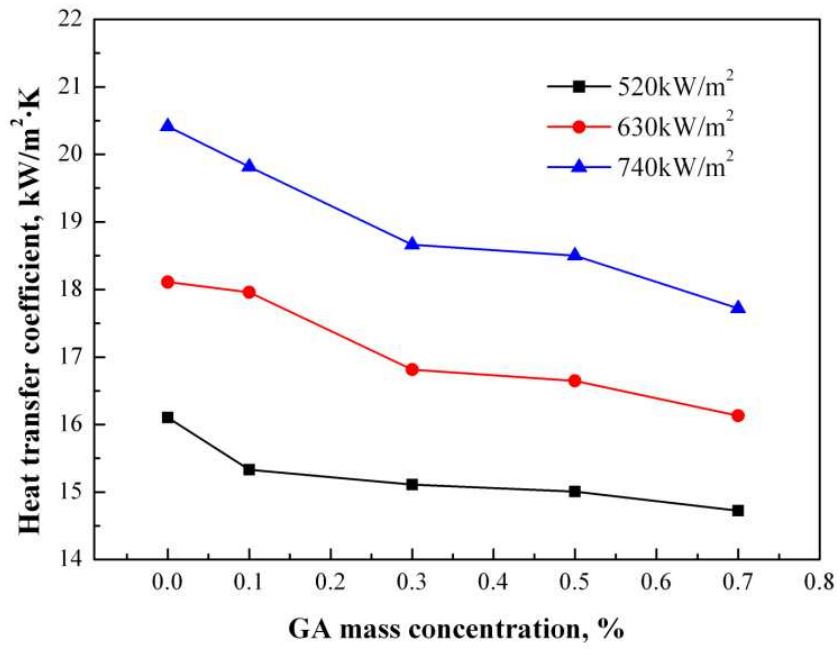


**Fig. 10.** Variation of the boiling heat transfer coefficient with the mass concentration of surfactant GA at three different heat fluxes of 520 kW/m<sup>2</sup>, 630 kW/m<sup>2</sup> and 740 kW/m<sup>2</sup>.

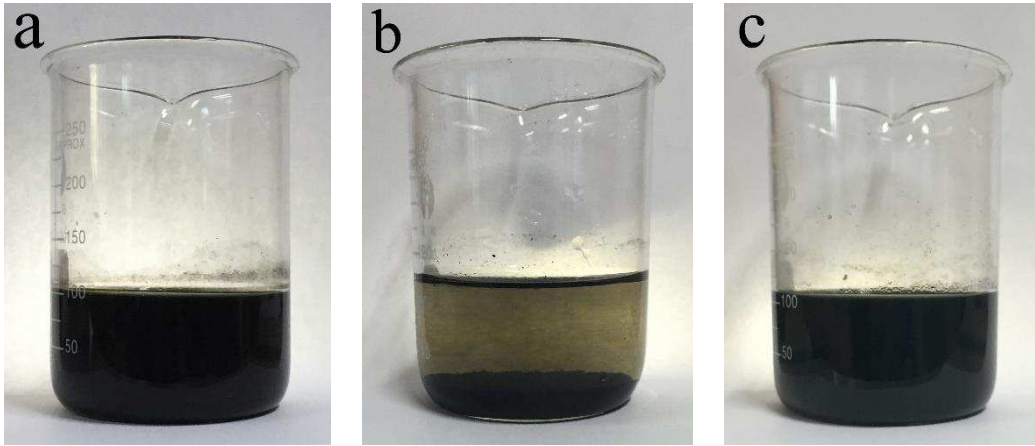


**Fig. 11.** Agglomeration condition of the MWCNTs nanofluids: (a) before boiling, (b) without GA after boiling, (c) with GA after boiling.



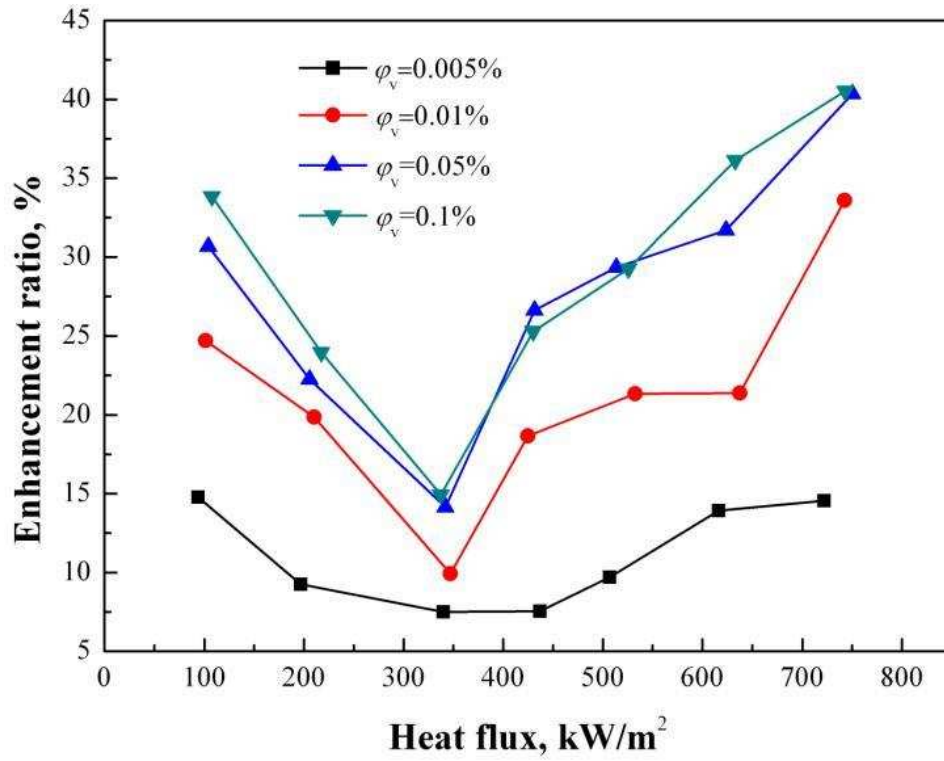
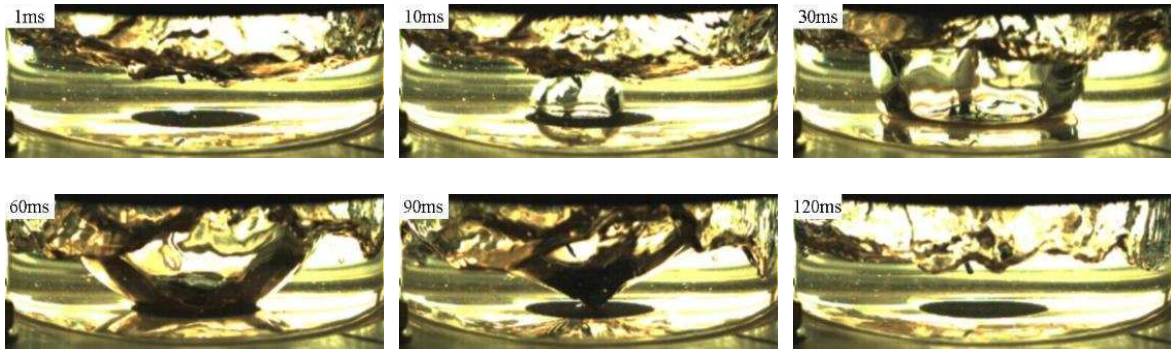
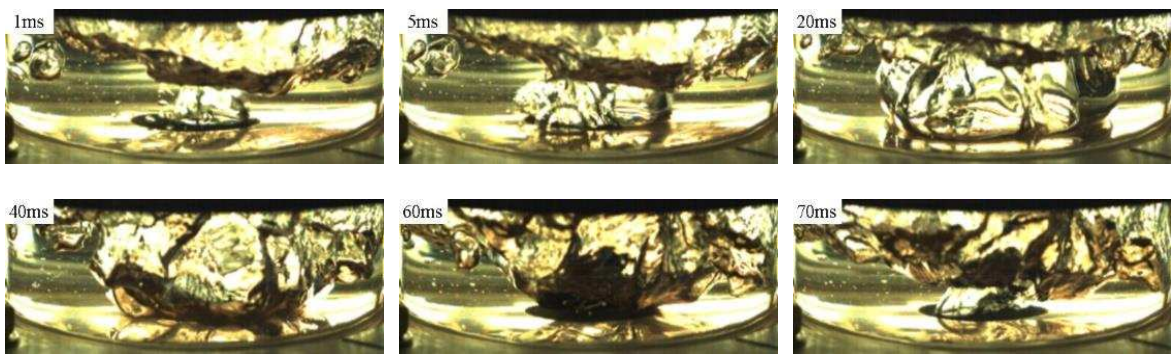


**Fig. 12.** Variation of the boiling heat transfer coefficient enhancement ratios of the MWCNTs nanofluids with the heat flux for four different volume fractions of 0.005%, 0.01%, 0.05% and 0.1%.



(a)



(b)

**Fig. 13.** Photographs of the bubble generation, growth and departure on the boiling surface with the MWCNTs deposition at two heat fluxes: (a)  $100\text{kW/m}^2$  and (b)  $740\text{kW/m}^2$ .